Void and grain resonances in discontinuous silver thin films close to the percolation threshold

2000 J. Phys.: Condens. Matter 12 4125

(http://iopscience.iop.org/0953-8984/12/17/316)

J. Phys.: Condens. Matter **12** (2000) 4125–4139. Printed in the UK PII: S0953-8984(00)10278-4

Void and grain resonances in discontinuous silver thin films close to the percolation threshold

A Da Silva†, C Andraud†, J Lafait† and A Dakka‡

† Laboratoire d'Optique des Solides de l'Université Pierre et Marie Curie, Unité Mixte de Recherche CNRS 7601, Case 80, 4, place Jussieu, 75252 Paris Cédex 05, France
‡ Laboratoire de Physique des Matériaux de l'Université Mohammed V, Faculté des Sciences, Avenue Ibn Batouta, BP 1014 Rabat, Morocco

E-mail: adasilva@ccr.jussieu.fr

Received 13 December 1999, in final form 28 February 2000

Abstract. An optical study of discontinuous metallic thin films has permitted us to observe simultaneously two resonant phenomena in media close to the percolation threshold. In addition to the well known metal grain resonance, a weaker resonance appears in the UV spectrum. This phenomenon, the presence of both resonances in a single sample, has seldom been pointed out. We demonstrate experimentally, on a silver percolating film, that this resonance is due to the presence of voids in the thin metal layer. We introduce a new model for the calculation of the optical properties of heterogeneous media, based on an entropic analysis of the actual medium, which accounts fairly well for both phenomena.

1. Introduction

Morphology governs the physical properties of heterogeneous materials and in particular the optical properties of granular metallic films [1]. According to the theories of Shannon and Brillouin [2, 3], developed in the 1950s, the morphology of a medium can be analysed in terms of quantity of information. This quantity is characteristic of the disorder of an image and is related to the statistical state of the configuration, in particular the entropy. We have adapted these information and entropy concepts to the image analysis of random two-phase media [4, 5] and developed a new tool of morphological characterization of the disorder of actual heterogeneous media: the normalized configuration entropy [6].

The analysis of different kinds of image of the morphology of simulated or actual two-phase media leads us to define a length, the optimal length l_0, characteristic of the disorder in the image. We concluded, following basic arguments, that it is at the scale l_0 that the calculation of the local properties of the medium is relevant.

In this context, we have developed a new model for the calculation of the effective dielectric function of a two-phase medium, which takes into account its exact morphology. Classical effective medium theories (EMTs) [7–10] account for the morphology, essentially by two global parameters: the fraction of the components and a depolarizing factor accounting for the average shape of the clusters. This is moreover the principal reason why they are unable to give a good account of the percolation in two-phase media. None of these models use any local parameters of the actual morphology of the medium, and they consequently cannot account for

0953-8984/00/174125+15$30.00

optical properties resulting from local fluctuations in the morphology of actual experimental media.

Our entropic model is based on a classical EMT for the local calculation of the dielectric functions, but, unlike them, it takes into account the medium morphology, by analysing actual images. In this sense, our method is close to the renormalization model based on the Kadanoff block theory [11]. It differs however in the details of the averaging procedure and in the fact that we determine a relevant scale for the local calculations. Both entropic and renormalization models have no free parameters, and can account for the optical properties of granular metallic films near the percolation.

In this paper, we will demonstrate the ability of the entropic model to account for a phenomenon seldom pointed out in these films: the simultaneous observation in the reflectance, transmittance and absorption spectra of the grain *and* void resonances. In fact, if the grain resonance on one hand and the void resonance [12–15] on the other hand have been separately observed for metal fraction respectively below and above the percolation threshold, we noticed that close to the percolation threshold the two resonances are present. We have observed and characterized the void resonance, reciprocal to the surface plasmon resonance in the metallic grains [13, 15], in discontinuous silver films just above the percolation.

In section 1, we briefly review the normalized configuration entropy and the principle of our model. Using simulated images, we compare the optical prediction of our model to those of the classical EMTs, i.e. Maxwell Garnett and Bruggeman theories. We focus our attention on the void resonance in images at and beyond the percolation threshold. In section 2, we apply the entropic analysis to an image, obtained via atomic force microscopy (AFM), of a granular silver film above the percolation threshold. We describe our experimental technique and present the results of the optical and morphological characterization of the discontinuous silver films that we have deposited. The third section is devoted to the discussion of the optical results: identification of the void resonance, and comparison with the entropic model.

2. Reminders about the entropic optical model

2.1. Normalized configuration entropy: $H^*(l)$

The morphological characterization has been developed with the aim of facilitating the evaluation of the optical properties of heterogeneous media. In this work we are concerned with granular silver films, for which the images have been partitioned in black (for metal) and white (for dielectric) pixels. The normalized configuration entropy [5, 16, 17] allows the determination of a relevant scale at which we decide to calculate the local optical properties of the medium.

This method consists of analysing a two-phase image through a sliding square window of variable size l, defining a set of l-cells (cells of size l). One then calculates the filling probability distribution $\{p_i\}$ of the image for each size l. The probability, $p_i(l)$, is defined as the number of l-cells containing i black pixels, $N_i(l)$, divided by the total number of l-cells, $N(l)$:

$$p_i(l) = \frac{N_i(l)}{N(l)}. \tag{1}$$

The advantage of a sliding window over a fixed grid is that it yields better statistics due to the larger number of samples. Applying then Shannon's entropy formula, we obtain the definition of the configuration entropy; the sum of each probability weighted by its own quantity

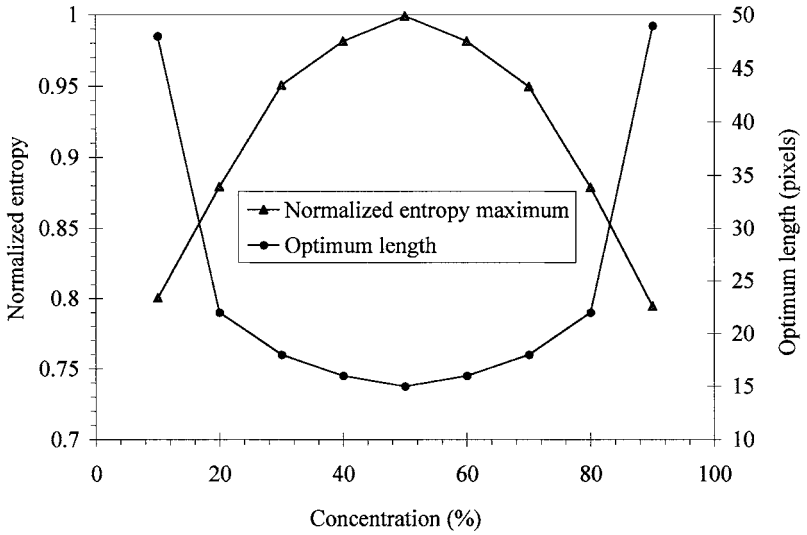

Figure 1. Evolution with the concentration of black pixels of the normalized entropy maximum and of the optimum length, on images generated by TBM.

of information (logarithm of the inverse probability):

$$H(l) = -\sum_{i=0}^{l^2} p_i(l) \ln[p_i(l)]. \tag{2}$$

In order to be able to compare entropy values calculated at different scales of analysis, it is necessary to normalize the entropy. For this normalization we have chosen, from theoretical considerations [2, 3, 5, 16, 17], the maximum theoretical entropy corresponding to the flat histogram of the filling probability distribution (all the probabilities being equal to the inverse of the number of possible occupations: $l^2 + 1$). We thus define the normalized configuration entropy as follows:

$$H^*(l) = \left(-\sum_{i=0}^{l^2} p_i(l) \ln[p_i(l)] \right) [\ln(l^2 + 1)]^{-1}. \tag{3}$$

We have applied our tool to different types of image, both experimental and simulated. It turns out, in all the cases that we have studied, that an optimum length l_0 exists, for which (1) the entropy is maximum; (2) the disorder is maximum; (3) the probability distribution is the closest to the flat histogram; (4) the highest number of different configurations is realized.

We can sum up these remarks as follows: the entropy optimum length l_0 is a characteristic of the disorder in the image; the larger the disorder is in the image, the smaller the optimum length. This optimum length reaches a minimum and the entropy a maximum near the percolation threshold [18], as it shows up in several images of variable concentration generated by different algorithms (figure 1). Around the percolation threshold, this minimum value of the optimum length corresponds to the size of the smallest constituent of the image—an element that, if randomly added, transforms the medium from the non-percolated to the percolated state.

At the size of the entropy optimum length, the maximum number of configurations can be observed, without redundancy or lack of information. From the point of view of optics, we consider that the local optical responses of all these different configurations will combine so

as to achieve the global optical response of the whole medium. This point of view is close to that of optical theories developed to account for the percolation [19, 20], except that we take into account the actual distribution function of the configurations at size l_0 in the image, as opposed to using the theoretical distribution given by percolation theory. Our optical model can therefore be applied to any morphology.

2.2. Local optical calculation

The entropic optical model [21] is thus based on local optical calculations performed after the partition of the image of the two-phase medium into blocks of size l_0 determined by the entropic analysis. One first calculates the metal fraction μ of each block, and determines its state of percolation by looking for a conducting path between two opposite edges of the block (using a four neighbour labelling). The effective dielectric function of each block is then calculated by using the generalized Maxwell Garnett model [7, 8]. In this model, a percolating block with metal fraction μ is replaced by an equivalent cell composed of a metallic matrix embedding a dielectric sphere with the dielectric fraction $(1-\mu)$; conversely, a non-percolating block is modelled by a dielectric matrix embedding a metallic sphere with the metal fraction μ. One thus obtains a series of effective dielectric functions of percolating (ε_{iP}) blocks (index i) and non percolating (ε_{kNP}) blocks (index k):

$$\varepsilon_{iP} = \varepsilon_M \frac{2\varepsilon_M + \varepsilon_D + 2(1-\mu_i)(\varepsilon_D - \varepsilon_M)}{2\varepsilon_M + \varepsilon_D - (1-\mu_i)(\varepsilon_D - \varepsilon_M)} \tag{4}$$

$$\varepsilon_{kNP} = \varepsilon_D \frac{2\varepsilon_D + \varepsilon_M + 2\mu_k(\varepsilon_M - \varepsilon_D)}{2\varepsilon_D + \varepsilon_M - \mu_k(\varepsilon_M - \varepsilon_D)}. \tag{5}$$

2.3. Global optical model

The model (inspired by Hilfer's model [22] for porous media) consists in performing a self-consistent calculation of the global effective dielectric function ε_E of the medium by using a Bruggeman model [9] generalized to N components (N is the number of blocks of size l_0 in the whole image). The polarizability resulting from the sum of all the components (blocks) embedded in the effective medium is set equal to zero in order to account self-consistently for the fact that, at first order, the heterogeneous cells do not scatter light when immersed in the equivalent effective homogeneous medium:

$$\underbrace{\sum_i \lambda_P^i \frac{\varepsilon_{iP} - \varepsilon_E}{\varepsilon_{iP} + 2\varepsilon_E}}_{\substack{\textit{Sum} \text{ on the} \\ \text{percolating blocks}}} + \underbrace{\sum_k \lambda_{NP}^k \frac{\varepsilon_{kNP} - \varepsilon_E}{\varepsilon_{kNP} + 2\varepsilon_E}}_{\substack{\textit{Sum} \text{ on the non-} \\ \text{percolating blocks}}} = 0 \tag{6}$$

where λ_P^i and λ_{NP}^i are the fractions of percolating and non-percolating blocks with metal fractions μ_i and μ_k.

We then calculate the optical properties R (reflectance), T (transmittance) and

$$A = 1 - R - T \tag{7}$$

(absorption) of the whole medium, by using the Abelès formulas [23] for thin films.

2.4. Prediction of grain and void resonances on simulated images

We now apply the entropic model to simulated images of a two-phase, metal–dielectric, medium, with the aim of pointing out the absorption peaks around the percolation. We chose silver as the metal (for which the dielectric function is modelled by a Drude function), and air

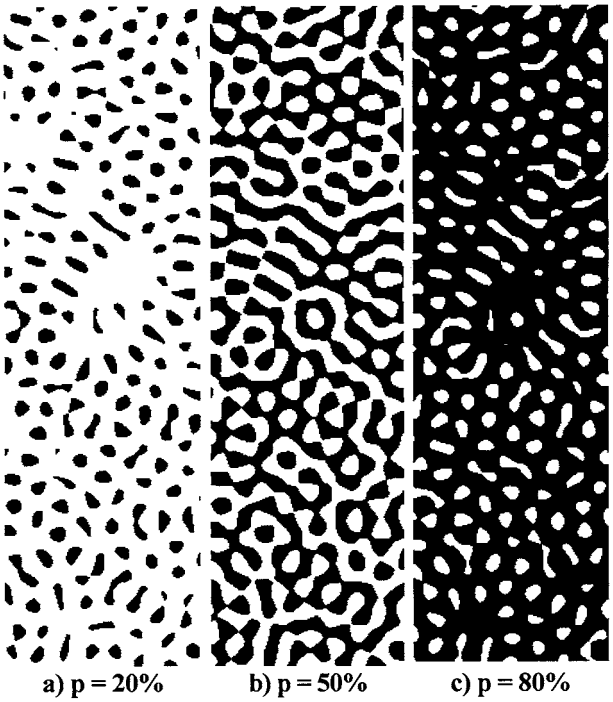

Figure 2. Images generated by TBM with different black pixel concentration.

as the dielectric ($\varepsilon_D = 1$). The images (figure 2) are generated by the turning band method (TBM) [24], with a cardinal sine correlation function. Different thresholdings allow us to obtain different black pixel (metal phase) fractions in the image.

In figure 3, we present the optical absorption curves for three metal fractions: 20% (below the percolation threshold p_c), 50% (just at the percolation threshold p_c for this type of image) and 80% (above p_c), as calculated by our model and by EMTs, i.e. the Maxwell Garnett model, the Maxwell Garnett model generalized by Cohen [8] (which we call Maxwell Garnett inverted) and the Bruggeman model.

Below the percolation threshold (figure 3(a)), our model predicts, like the Maxwell Garnett model, the metallic grain resonance at 380 nm. Above the percolation threshold (figure 3(c)), it predicts, like the Maxwell Garnett inverted model, the void resonance at 330 nm and some extra absorptions. The latter may be due to the combined contributions of Maxwell Garnett and Bruggeman models as applied to pseudo-random images. These extra structures might not be observed in actual media.

At the percolation threshold (figure 3(b)), the Maxwell Garnett model still only predicts the metallic grain resonance, while the Maxwell Garnett inverted model still only predicts the void resonance. The Bruggeman model shows a broad absorption covering the whole domain of the resonances. Our model, on the other hand, shows the simultaneous presence of the void resonance *and* the grain resonance. The latter appears on the left edge of a broad absorption analogous to Bruggeman's one.

The void resonance has been named by analogy with the grain resonance [13, 15]. In fact, since the grain resonance results from the excitation of a surface plasmon mode of the conduction electrons in the spherical silver grains, the void resonance is explained by the fact

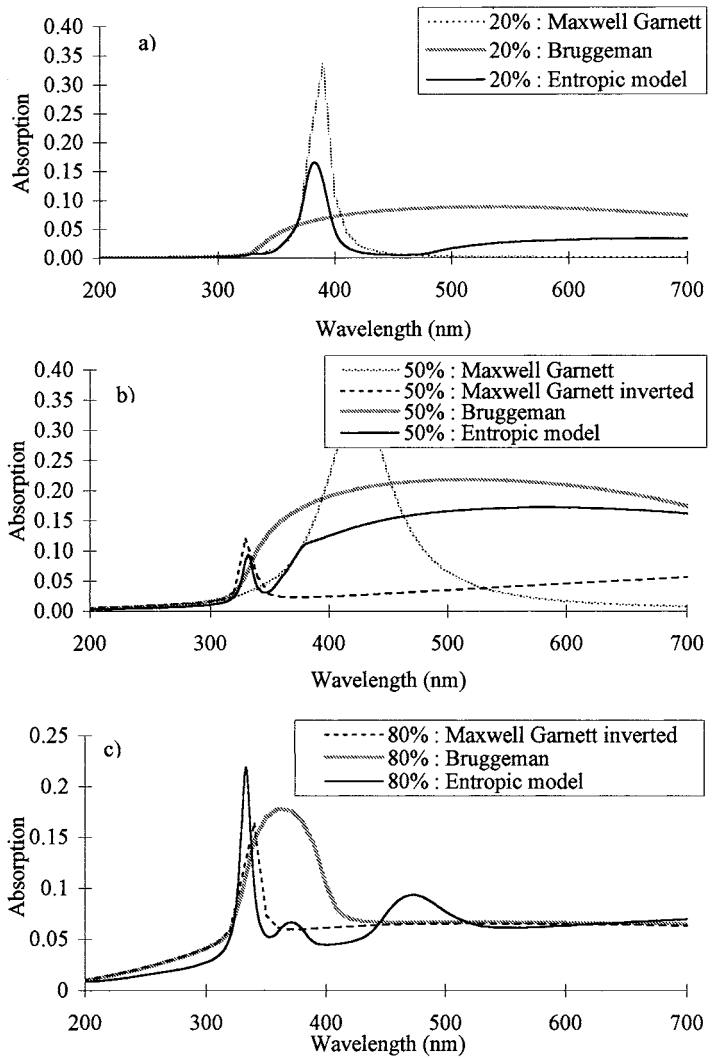

Figure 3. Absorption curves of different images generated by TBM for different black pixel fractions: (a) $p = 20\%$; (b) $p = 50\%$; (c) $p = 80\%$. Comparison between our model and EMT.

that the metal conduction electrons surrounding a hollow of dielectric are also excited in a surface resonant mode. This reasoning allows us to express the polarizability α of a dielectric void embedded in a metallic medium by

$$\alpha = (1 - p)\frac{\varepsilon_D - \varepsilon_M}{\varepsilon_D + 2\varepsilon_M} \tag{8}$$

where p is the metal fraction, ε_D is the dielectric function of the dielectric and ε_M the dielectric function of the metal. This expression is an equivalent formulation for the polarizability of a unit cell (i.e. cell of volume 1) composed of a dielectric sphere of volume $(1 - p)$ embedded in a metallic medium.

This polarizability is then identified, according to the Maxwell Garnett model generalized by Cohen *et al* [8], to the polarizability of a unit cell composed of a 'hole', which is a sphere

of volume 1, of effective media embedding in a metallic medium,

$$\alpha = \frac{\varepsilon_E - \varepsilon_M}{\varepsilon_E + 2\varepsilon_M} \tag{9}$$

where ε_E is the effective dielectric function of the medium and ε_M the dielectric function of the metal.

Our model and the Maxwell Garnett models predict a weaker amplitude for the void resonance than for the metallic grain resonance. An asymmetry effectively shows up in formulas (8) and (9) explaining this discrepancy. At the microscopic scale, one may infer as an explanation, that the conduction electrons may be less confined around the interface surface for the dielectric cavities than in the case of metallic grains.

3. Experimental techniques, optical and morphological results

3.1. Granular film deposition

In order to be able to observe both the void and the grain resonances, we have deposited granular silver films close to the percolation threshold. Silver is the most interesting noble metal for this observation. Indeed, the positions of those two resonances are expected to be located out of the interband transition domain. In gold films, for example, the void resonance, weak absorption expected around 400 nm, should be smeared in the interband absorption, predominant below 650 nm.

We have taken AFM images of the morphology (in order to apply our model) and measured their optical properties.

Our films were deposited by thermal evaporation under ultra high vacuum (approximately 10^{-8} Torr), with a deposition rate close to 0.05 nm s^{-1}, on fixed silica substrates positioned 40 cm above the heated crucible.

The mass thickness d_m (thickness of a continuous film with equivalent mass) is evaluated by using a quartz oscillator. We report here the results concerning the most demonstrative film with a mass thickness $d_m = 11$ nm.

3.2. Optical properties

The optical measurements (reflectance R and transmittance T) were performed using a Cary 5 double-beam spectrophotometer, under near normal incidence, in the spectral range of 200–2500 nm (figure 4). With this instrument, we obtain an absolute measurement of R and T, with data intervals of 0.5 nm (we can estimate the spectral accuracy of the measurement to be ± 0.5 nm).

The behaviour of the experimental optical properties of the sample in the near infrared (beyond 700 nm), gives some qualitative information about its percolation state: the increasing reflectance R and the decreasing transmittance T as we increase toward large wavelengths are characteristic of the metallic behaviour of the whole medium. Our results indicate that this sample is well beyond the percolation.

Below 300 nm, the optical properties are dominated by the absorption caused by the silver interband transitions. We explain in section 3 how we take into account this contribution.

Between 300 nm and 700 nm, the behaviour is resonant-like. The absorption peak centred near 400 nm corresponds to the surface plasmon resonance in metallic grains. One may notice the simultaneous presence, near 350 nm, of another resonance, less intense, that we attribute to the presence of voids in the metal. This particular resonance is more easily remarked in

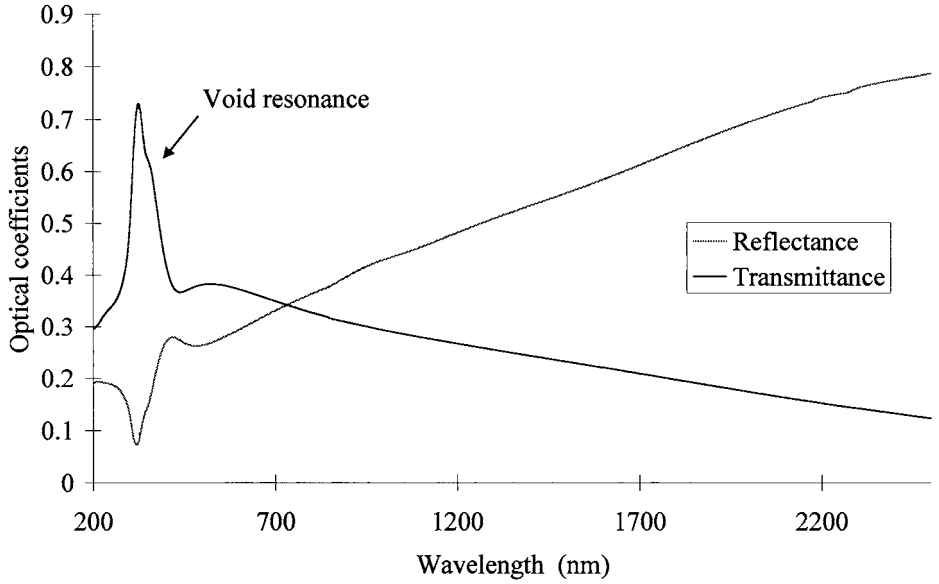

Figure 4. Reflectance and transmittance curves of a granular silver film with a silver layer thickness $d_m = 11$ nm.

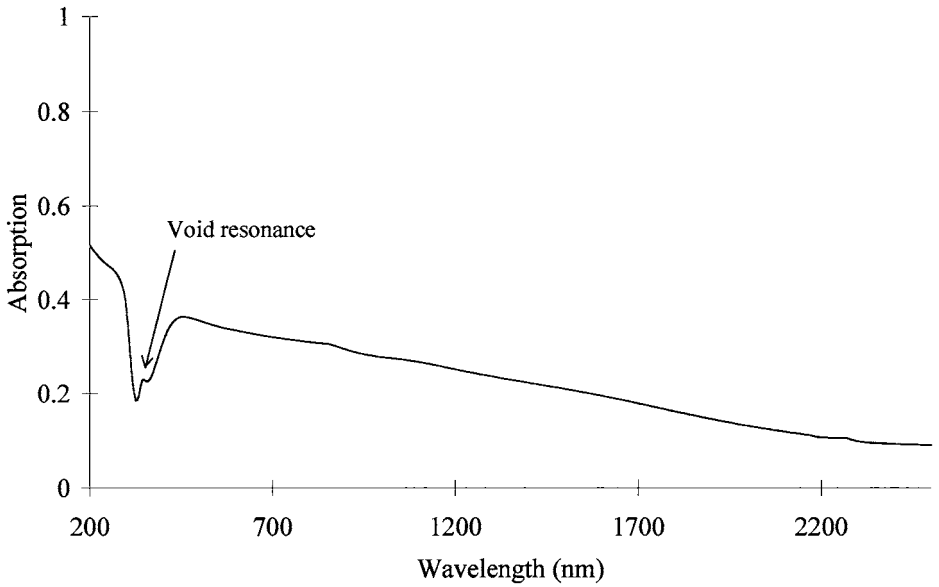

Figure 5. Absorption curve of a granular silver film with a mass thickness $d_m = 11$ nm.

the absorption curves (figure 5). The absorption curve of another sample (figure 6), below the percolation ($d_m = 7$ nm), exhibits a similar feature around 350 nm, in the form of a very weak shoulder. This effect is so weak that we have not tried to simulate it. This behaviour may be explained by the fact that the geometries below and above the percolation are not exactly symmetrical. Below the percolation threshold, for instance, few resonance producing

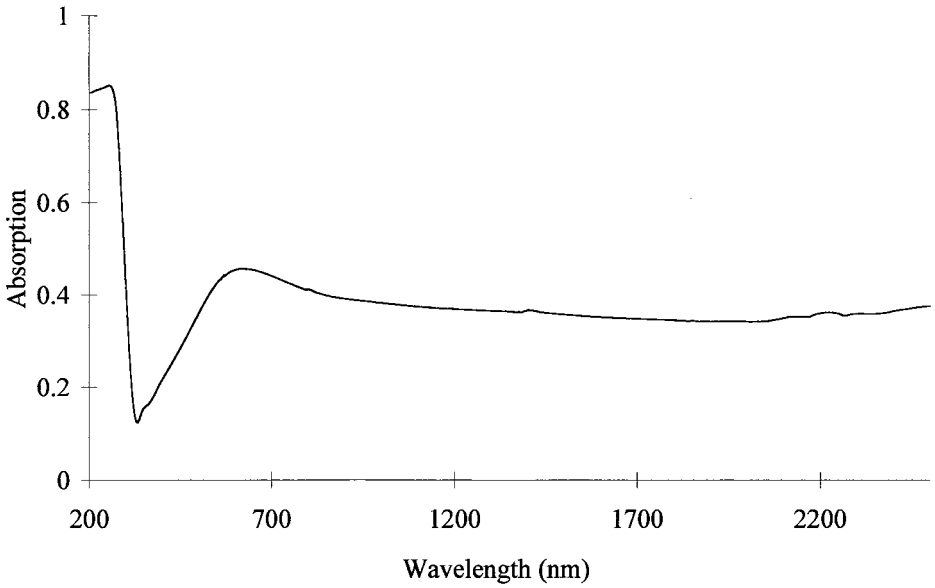

Figure 6. Absorption curve of a granular silver film with a mass thickness $d_m = 7$ nm.

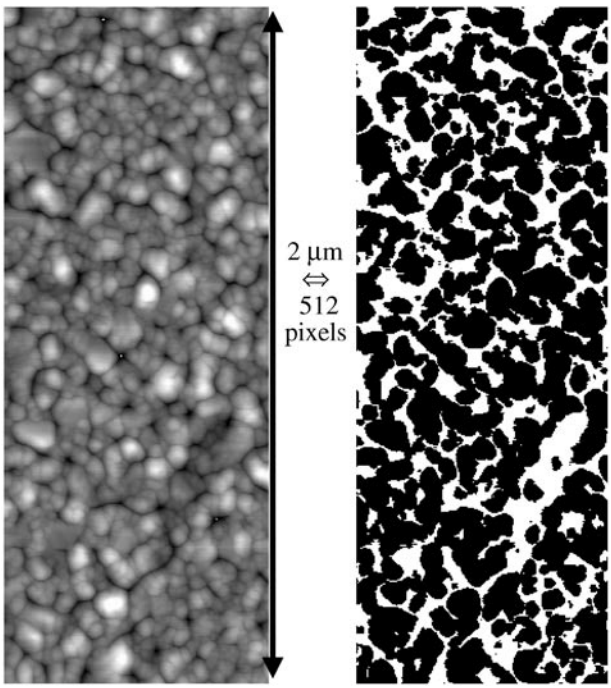

Figure 7. AFM image of a granular silver film ($d_m = 11$ nm) and its binarization in black and white pixels ($p = 69\%$).

voids with roughly spherical shape can be observed. Above the percolation threshold on the other hand, one can observe the coexistence of both voids and metal clusters with roughly

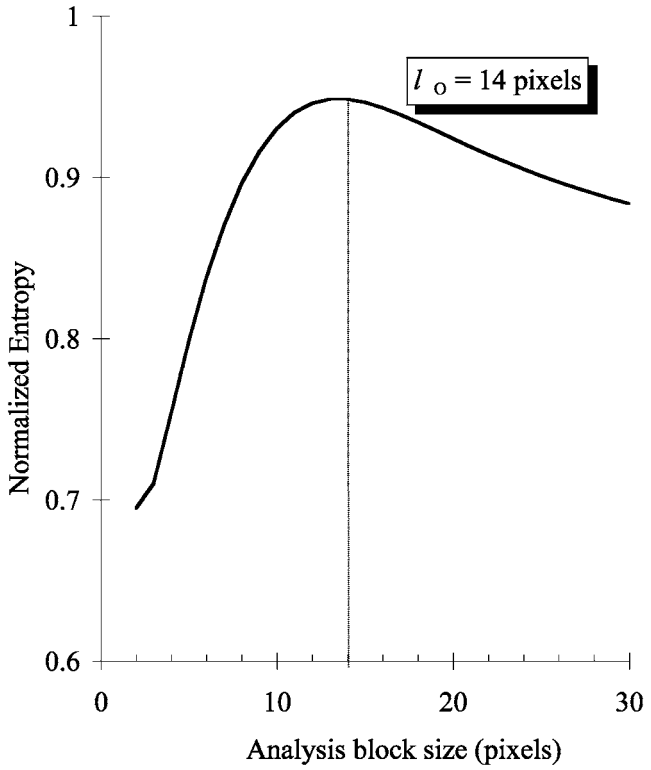

Figure 8. Determination of the optimal length for an image of an actual media: a granular silver film with $d_m = 11$ nm and $p = 69\%$.

spherical shape. We have tried to 'prove' experimentally that the extra absorption observed in a percolating medium is due to a void resonance by changing the dielectric constant of the hollow itself (see section 3).

3.3. Entropic analysis of the morphology

We took images (2 μm $\times$ 2 μm) of our sample by atomic force microscopy (AFM) in contact mode with a resolution of 512 $\times$ 512 pixels. They were filtered and binarized (black pixels for the metal and white for the dielectric) using a thresholding method developed in our laboratory (figure 7), in order to distinguish between the two phases present in this kind of image, without information loss. This method allows us to determine the metal fraction in the image, $p = 69\%$, and the mean physical thickness of silver in our sample, $d \approx d_m/p = 16$ nm.

As mentioned in section 1, as a first step of the entropic model, we perform the entropic analysis of this image by exploring it with a square-sliding window of variable size, l. One thus obtains the normalized configuration entropy curve (figure 8). From the position of the maximum of $H^*(l)$, one obtains a characteristic length of $l_0 = 14$ pixels corresponding to 54.7 nm.

It is at this discretization size that the local optical properties will be calculated, using a sliding window technique.

4. Comparison with the entropic model and discussion

In previous articles, we have demonstrated that our model accounts well for the infrared properties and the grain resonance of granular metallic films. Our aim is now to account for the void resonance located in the ultraviolet. For this reason we focus on the results in the corresponding wavelength range, extended to the domain of the metallic grain resonance.

4.1. Entropic model applied to the film as deposited

In order to apply our model, we first need to know the dielectric functions of the two components of the medium. The silver dielectric function (having real $\varepsilon_1(\omega)$ and imaginary $\varepsilon_2(\omega)$ parts) is modelled by a Drude function ($\varepsilon_1^0(\omega)$ and $\varepsilon_2^0(\omega)$), for which the contribution of the interband transitions ($\varepsilon_1^{i.b.}(\omega)$ and $\varepsilon_2^{i.b.}(\omega)$) is added:

$$\begin{aligned}\varepsilon_1(\omega) &= \varepsilon_1^0(\omega) + \varepsilon_1^{i.b.}(\omega)\\ \varepsilon_2(\omega) &= \varepsilon_2^0(\omega) + \varepsilon_2^{i.b.}(\omega).\end{aligned} \tag{10}$$

The Drude dielectric functions are written:

$$\varepsilon_1^0(\omega) = P - \frac{\omega_p^2}{(\omega^2+\omega_\tau^2)}$$

$$\varepsilon_2^0(\omega) = \frac{\omega_p^2\omega_\tau}{\omega(\omega^2+\omega_\tau^2)}$$

and are parametrized by an electronic polarization, P (considered as a constant from the UV to near infrared), a plasma frequency of the conduction electrons, ω_p, and ω_τ, a term related to the relaxation time of electrons. This last term has been corrected from the classical size effect by taking into account the mean radius of the particles. Indeed, $\omega_\tau = \omega_{\tau b} + \omega_{\tau F}$ where $\omega_{\tau b}$ is the contribution of the bulk material, proportional to $1/\tau$ (τ is the relaxation time of electrons), and $\omega_{\tau F}$ is a correction due to the finite size of the particles, proportional to v_F/L (v_F denoting the Fermi velocity of the electrons and L the mean free path depending on the particle size).

We have determined the Drude parameters and the interband transition dielectric function of the silver grains. P, ω_p and $\omega_{\tau b}$ have been deduced by fitting the dielectric function determined from optical measurements on a thick silver sample. We obtained $P = 3.5$, $\hbar\omega_P = 9.5$ eV and $\hbar\omega_{\tau b} = 0.06$ eV. The correction on ω_τ is $\hbar\omega_{\tau F} = 0.14$ eV for a mean diameter of particles equal to 38 nm.

The dielectric in the present case is air ($\varepsilon_D = 1$). Its dielectric function does not vary with the wavelength. One may notice, however, that our problem is a two-dimensional one: indeed, as the silver layer is thin enough (11 nm) and the particle size is of the same size, one may assume that the discontinuous film is a 2D distribution of grains on the substrate. Therefore, the electrostatic (or better, electromagnetic) interaction between the grains and the substrate should be taken into account in the model. It is usual [25–27] to consider that a very first and simple step of this account is to attribute to the index of the matrix embedding the grains an intermediate value between air ($\varepsilon_D = 1$) and substrate ($\varepsilon_D = 2.25$). Therefore, we chose $\varepsilon_D = 1.5$.

If we compare the absorption curve obtained by our model (with a step of calculation of 2 nm) to the experimental one (figure 9), one first remarks that the void resonance of the theoretical curve (at 345 ± 2 nm) fits quite well the void resonance in the experimental curve (at 347.0 nm $\pm$ 0.5 nm), with respect to both width and amplitude. Nevertheless, the model predicts an overall absorption curve weaker than the experimental one. This can be attributed to a basic underestimation of the grain interactions in the model, due to the fact that an average

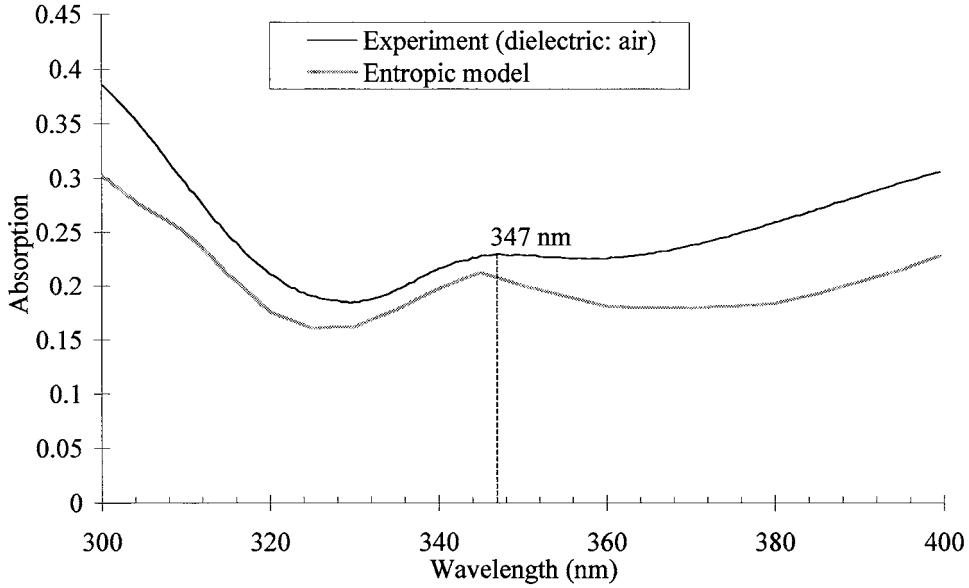

Figure 9. Comparison between the absorption curve measured and the modelled one for a granular silver film with $d_m = 11$ nm and $p = 69\%$.

(even if self-consistent) of the optical response of the cells of size l_0 is made which does not take into account the interactions between cells.

4.2. Another dielectric: glycerin

In order to identify more unambiguously this void resonance, we have tried to demonstrate experimentally that its properties depend directly on the index of refraction of the dielectric cavity, by replacing the air, initially filling the voids, by another medium. In the model, the wavelength of the void resonance is fixed by the vanishing of the real part of the denominator of the 'void dipole'

$$\varepsilon_1 = \frac{-p}{3-p}\varepsilon_D \tag{11}$$

where ε_1 is the real part of the Drude function with the contribution of the interband transitions, ε_D is the dielectric constant and p is the metal fraction in the image.

If ε_D increases from 1.5 to 2.25, the model predicts a 2 nm shift of the resonance towards higher wavelengths.

The embedding medium we needed should present the following characteristics:

(i) a refractive index as high as possible;
(ii) be non-absorbing in the UV wavelength range;
(iii) have an intermediate viscosity coefficient, not too high (in order to fill the 'voids'), and not too low (so that it remains in the film during the spectrophotometer optical measurements).

We finally chose glycerin, even though this substance has some UV absorption. We measured the optical properties of a sample obtained by introducing a glycerin layer between two silica substrates. We effectively observed a weak absorption, nearly constant in the UV wavelength range (figure 10). We determine an extinction coefficient constant of $k = 10^{-5}$, by

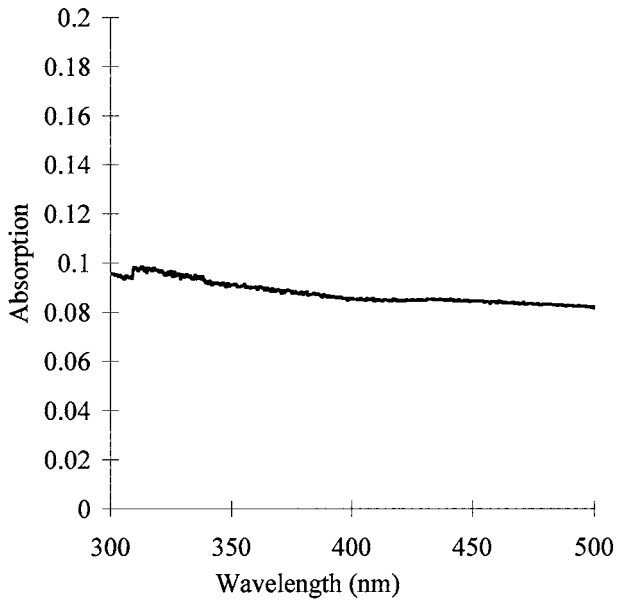

Figure 10. Absorption curve measured for a layer of glycerin between two substrates of silica.

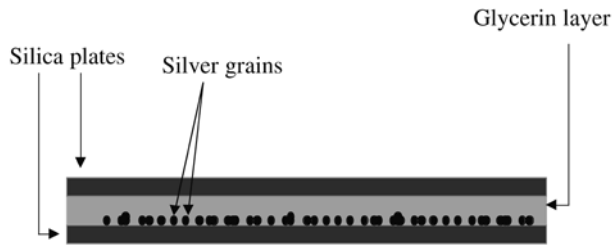

Figure 11. Scheme of the modelled system.

assuming that in this spectral range the real part of the refractive index is equal to its theoretical value 1.49, taken from the literature [28], and by fitting the layer thickness at 220 μm.

A layer of glycerin was then put on our discontinuous silver film, which was then covered with a silica plate in order to stop the flow of glycerin (figure 11). We observed the wavelength shift predicted by the model (figure 12), even if the slight discrepancy (around 2 nm) already observed with the air matrix between the positions of the experimental resonance and the calculated one still remains here. In table 1, we summarize the results for the void resonance wavelength given by the experimental curve, by our model and by the EMT formula (11) and determined by a local derivation method. The spectral accuracy of the determination of these maxima is given on one hand by the spectral resolution of the measurement, and on the other hand by the spectral step of our calculation.

The EMT formula and our model predict the same wavelength shift, even though they do not position the resonance at the same wavelength (in our model, a preliminary mean is performed on every cell at the size l_0, before effective medium averaging on these cells, whereas in the EMT formula an averaging is performed over the whole medium). Nevertheless, we notice that the void resonance is now located at 348 nm when we expected it at 347 nm, since the

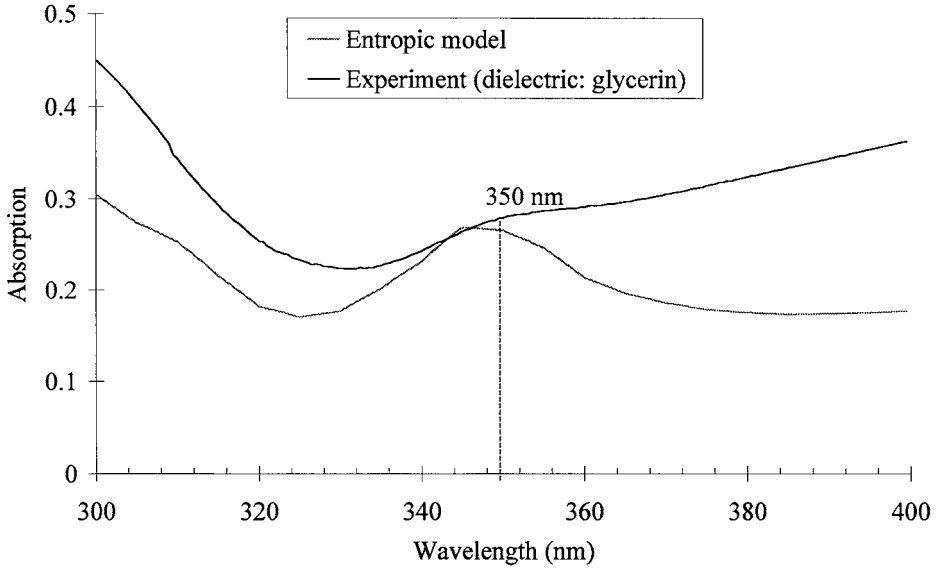

Figure 12. Shift of the void resonance.

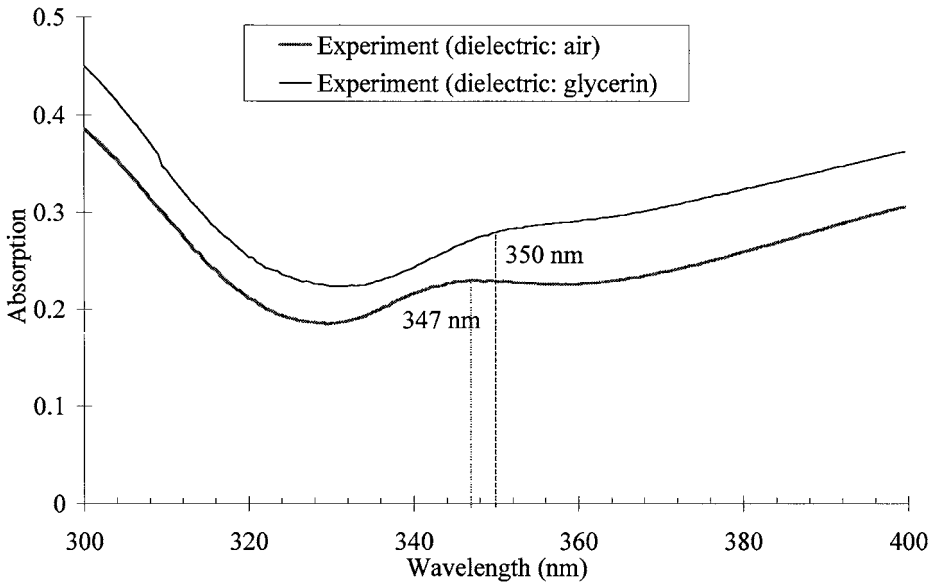

Figure 13. Comparison between the absorption curve measured and the modelled one for a granular silver film with $d_m = 11$ nm and $p = 69\%$, where air was replaced by glycerin.

EMT formula predicts a shift of 2 nm. If we consider the error factor in the determination of the volume fraction of the metal in the layer, we can assume that our model predicts quantitatively this shift due to the nature of the dielectric.

The curve in figure 13 depicts a medium globally more absorbing than that of figure 9. This is probably due in part to the fact that some silver grains may have been shifted or carried away by the application of the glycerin. However, if we compare the model and the experimental

Table 1. Position of the void resonance given by the experimental absorption curve, by our model and by the EMT formula.

	Position of the void resonance (nm)		
Dielectric medium	Experiment	Entropic model	EMT
Air	347.0 ± 0.5	345 ± 2	345
Glycerin	350.0 ± 0.5	348 ± 2	347

curves, we notice that our model predicts an amplification of the intensity of the void resonance. It is also possible that we underestimated the glycerin index and/or the thickness of its layer.

5. Conclusion

Our optical model based on an entropic analysis of the actual morphology of granular films was successfully applied to the prediction of the optical properties of discontinuous silver films above the percolation. It gave a fair account of the position of two resonant absorptions simultaneously observed in these media: the metallic grain resonance and the void resonance, and their modification when the index of the dielectric is experimentally changed by embedding the film in a glycerin layer.

References

[1] Jarett D N and Ward L 1976 *J. Phys. D: Appl. Phys.* **9** 1515
[2] Shannon C 1948 *Bell. Syst. Tech. J.* **27** 623–56
[3] Brillouin L 1956 *Science and Information Theory* (New York: Academic)
[4] Beghdadi A, Andraud C, Lafait J, Peiro J and Perreau M 1993 *Fractals* **1** 671–9
[5] Andraud C, Beghdadi A and Lafait J 1994 *Physica* A **207** 208–12
[6] Andraud C, Lafait J and Beghdadi A 1998 *Phys. Rev.* B **57** 13 227–34
[7] Maxwell Garnett J C 1904 *Phil. Trans. R. Soc.* A **203** 385
[8] Cohen R W, Cody G D, Coutts M D and Abeles B 1973 *Phys. Rev.* B **8** 3689
[9] Bruggeman D A G 1935 *Ann. Phys.* **24** 636
[10] Sheng P 1980 *Phys. Rev. Lett.* **45** 60
[11] Berthier S, Lafait J and Driss-Khodja K 1987 *Europhys. Lett.* **4** 1415
[12] Galeener F L 1971 *Phys. Rev. Lett.* **27** 421–23
Galeener F L 1971 *Phys. Rev. Lett.* **27** 1716–19
[13] Stroud D 1979 *Phys. Rev.* B **19** 1783–91
[14] Cummings K D, Garland J C and Tanner D B 1984 *Phys. Rev.* B **30** 4170–82
[15] Shalaev V M 1996 *Phys. Rep.* **272** 61–137
[16] Beghdadi A *et al* 1994 *Fractals in Natural Sciences* ed T Viscek, M Schlesinger and M Matsushita (Singapore: World Scientific)
[17] Blacher S, Brouers F and Van Dyck R 1993 *Physica* A **197** 516
[18] Andraud C *et al* 1997 *Physica* A **235** 307
[19] Yagil Y *et al* 1991 *Phys. Rev.* B **43** 11 342
[20] Robin T and Souillard B 1993 *Physica* A **193** 79
[21] Andraud C, Lafait J, Beghdadi A and Peiro J 1997 *Proc. Int. Conf. ETOPIM 4 (Moscow, 1996)* ed A Lagarkov (*Physica* A **241** 133)
[22] Hilfer R 1991 *Phys. Rev.* B **44** 60
[23] Abelès F 1967 *Advanced Optical Techniques* ed A C S Van Heel (Amsterdam: North-Holland) p 143
[24] Matheron G 1972 *Adv. Appl. Prob.* **5** 439
[25] David E 1939 *Z. Phys.* **114** 389
[26] Doremus R H 1964 *J. Chem. Phys.* **40** 2389
Doremus R H 1965 *J. Chem. Phys.* **42** 414
Doremus R H 1966 *J. Appl. Phys.* **37** 2775
[27] Yoshida S, Yamaguchi T and Kinbara A 1972 *J. Opt. Soc. Am.* **62** 1415–19
[28] 1963 *American Institute of Physics Handbook* 2nd edn (McGraw-Hill) pp 6–90